Optical Engineering

SPIEDigitalLibrary.org/oe

Shift-multiplexing complex spectral-domain optical coherence tomography

Haochong Huang
Zhuqing Jiang
Dayong Wang
Wenyuan Cai
Tianlong Man
Zhe Wang
Spozmai Panezai

SPIE

Shift-multiplexing complex spectral-domain optical coherence tomography

Haochong Huang,[a,b] Zhuqing Jiang,[a,b,*] Dayong Wang,[a,b] Wenyuan Cai,[a,b] Tianlong Man,[a,b] Zhe Wang,[a,b] and Spozmai Panezai[a,b]
[a]Beijing University of Technology, College of Applied Sciences, Beijing 100124, China
[b]Beijing University of Technology, Institute of Information Photonics Technology, Beijing 100124, China

Abstract. We propose and experimentally demonstrate a shift-multiplexing complex spectral-domain optical coherence tomography (shift-multiplexing CSD-OCT) method, in which the maximum detection depth of SD-OCT can be greatly extended by incorporating the shift-multiplexing of detection positions with CSD-OCT. The tomographic imaging with twofold or threefold microscopic slides as the target sample is performed. The experimental results show that the tomographic imaging with more uniform brightness and clarity for the different depth regions in a thick sample can be achieved by the shift-multiplexing CSD-OCT system. In particular, even while the sample's depth is beyond the maximum imaging depth of CSD-OCT system, the tomographic imaging of this sample can still be realized by using the shift-multiplexing CSD-OCT method without the need for any replacement of the equipment, such as high spectral capacity grating or high resolution of CCD. The shift-multiplexing CSD-OCT system can perform the imaging with the optimization and less reduction of sensitivity for the deeper detection position in the sample. [DOI: 10.1117/1.OE.53.1.014101]

Keywords: optical coherence tomography; spectral-domain optical coherence tomography; phase shift; measurement method; image detection system.

Paper 131017 received Jul. 8, 2013; revised manuscript received Nov. 11, 2013; accepted for publication Dec. 2, 2013; published online Jan. 3, 2014.

1 Introduction

Optical coherence tomography (OCT) is an advanced optical imaging technique that can be applied in imaging biological tissue due to its noncontact and noninvasive high-resolution capabilities for the semitransparent objects. Soon after its first application, OCT became an effective medical diagnostic and imaging tool in various fields of medicine, including ophthalmology, cardiology, tumor margining, etc.[1,2]

Spectral-domain optical coherence tomography (SD-OCT) is an OCT modality based on the Michelson interferometer and the spectrometer. The light beam from a super luminescent diode (SLD) source is divided into an object beam and a reference beam via the beam splitter. After the object beam is backscattered by a target sample at the end of the sample arm and the reference beam is reflected by a mirror at the end of the reference arm, the same spectral components of two beams will interfere to form the spectral interference fringes containing the depth information of the sample. After having performed the inverse Fourier transform of the spectral interference fringe, the tomographic image with the depth information of sample can be obtained.[1–7]

As it is known, SD-OCT system can acquire certain depth information of a sample without axial scanning by moving the reflection mirror or sample. As compared to time-domain OCT (TD-OCT), it does not need mechanical scanning in the axial direction, so it can be superior to the TD-OCT in data acquisition speed.[3] Even if SD-OCT has a lot of advantages, the depth-resolved imaging range of SD-OCT is limited due to the presence of the complex-conjugate image in tomographic imaging. The tomographic image and its complex conjugate are symmetrical on both sides of the direct current (DC) term in the entire image area due to Fourier transform, such that only a half of the depth range can be utilized. Thus, the spacing between the DC term and the left (or the right) edge on the tomographic image of SD-OCT actually determines its maximum detection depth $D_{\max}$. In order to overcome the limitation of SD-OCT, a complex SD-OCT (CSD-OCT) is introduced, in which the entire image area of tomographic imaging can be used to display depth information of the sample by the removal of the complex-conjugate image with the phase shifting method. The phase shifting method is a technique that makes use of a phase shifting mechanism and algorithm to eliminate the complex-conjugate image of tomographic imaging. Thus, its maximum detection depth is twice that of SD-OCT, that is $2D_{\max}$.[7–19] Still, the available imaging depth in CSD-OCT system is restricted by several factors, such as the grating spectral capacity, the resolution of the CCD, the coherence length of light source, and the optical properties of the sample.[4–6] The maximum detection depth of the SD-OCT system is actually dependent on the existing spectral capability of the spectrometer. Therefore, if the tomographic imaging is conducted in a high scattering sample that may cause a strong backscattered light or in a deeper detected position than $2D_{\max}$, it is necessary to enhance the depth imaging capability of the system by improving the experimental setup or introduce a new method.[6]

In this paper, we propose and demonstrate a new technique of shift-multiplexing CSD-OCT, in which the maximum detection depth of SD-OCT can be greatly improved by incorporating the shifted detection point with the removal

*Address all correspondence to: Jiang Zhuqing, E-mail: zhqjiang@bjut.edu.cn

of complex conjugate by a phase shifting method. The shift-multiplexing CSD-OCT system can achieve optimized imaging quality comparable to CSD-OCT without any system modification, such as high spectral capacity grating or high resolution of CCD. Moreover, the imaging sensitivity is gradually decreased as the sample moves away from the virtual image of the mirror in the sample path, i.e., the position of zero path difference;[6] that is why better tomographic imaging of a typical SD-OCT system should be carried out near the DC term. With our proposed shift-multiplexing CSD-OCT system, the above-mentioned high-sensitivity region of tomographic image can be actually made the most of, and thus it can perform optimized imaging with less reduction of sensitivity for the deeper detection position in the sample. The experiments are also performed to demonstrate the tomographic imaging performance of a shift-multiplexing CSD-OCT system.

2 Experimental Setup and Principle

The entire image area on both sides of the DC term can be used for imaging in CSD-OCT system because of the removal of complex-conjugate image with the phase shifting method. Our proposed shift-multiplexing CSD-OCT is mainly based on the CSD-OCT technique combined with regularly shifting of the primary detection locations in the axial direction to extend available detection range of sample.[20–25]

Figure 1 is a schematic diagram of the experimental setup of shift-multiplexing CSD-OCT. The shift-multiplexing CSD-OCT system is similar to the configuration of an SD-OCT based on Michelson interferometer with the exception of an additional translation stage at the sample arm. The light source in the system is a broadband SLD (S840 of Superlum Corporation, Ireland). The light emitted by an SLD source with a wavelength of 840 nm and spectral width of 70 nm is used. The detection arm consists of a spectrometer containing diffraction grating, a lens, and a CCD camera, which is gray-scale array CCD (GRAS-50S5M/C of PointGrey Corporation, Canada). The piezoelectric ceramic translation stage located at the end of the reference arm having a mirror mounted on it is used to make the phase shifting. In the sample arm, a translation stage is used to shift and position the primary detection points.

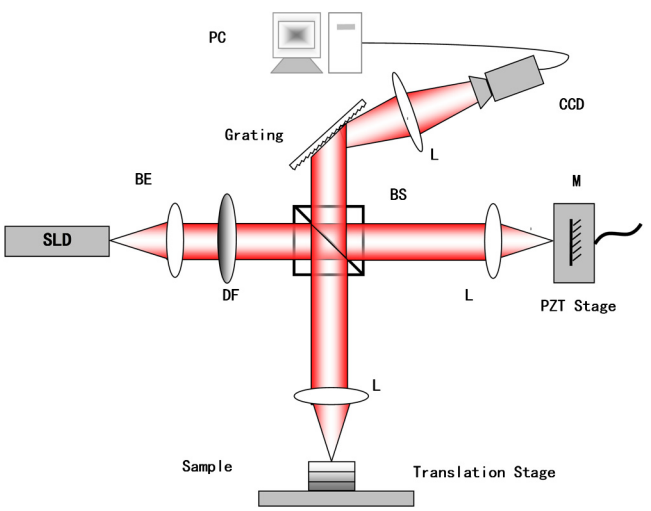

Fig. 1 The experimental setup of the shift-multiplexing complex spectral domain optical coherence tomography (CSD-OCT). SLD, super luminescent diode; BE, beam expander; DF, density filter; L, lens; BS, beam splitter; PZT stage, piezoelectric ceramic translation stage; M, mirror; CCD, charge coupled device; PC, personal computer.

In the shift-multiplexing CSD-OCT system, the position of the virtual image of the mirror imaging on the sample arm is defined as the primary detection position. The imaging depth range centered at the primary detection position is referred to as the effective detection range d, the value of which may be taken as less than or equal to the maximum detection depth $2D_{\max}$ of CSD-OCT. The tomographic imaging of the sample within the effective detection range d is conducted after locating each of the primary detection positions. With the movement of the sample stage in the axial direction, the primary detection position along the sample arm can be shifted and located one after another. The location of the mirror's virtual image relative to the sample depends on the optical path difference between the sample arm and the reference arm. The optical path length between the two adjacent primary detection positions is referred to as shift spacing Δd.

Figure 2 is a schematic diagram for illustrating the shift-multiplexing CSD-OCT scheme. The primary detection position is initially set near the first inner surface of the sample, shown as position A in Fig. 2; then by the movement of the sample stage with shift spacing Δd, the primary detection position can be changed sequentially to positions B and C, respectively. As the primary detection positions are located at different depths of the sample, such as positions A, B, and C, the interference images at the different depth segments are collected by CCD camera, respectively. Thus, by means of locating the primary detection position in sequential order or selectively, the tomographic imaging around the specified depth of the sample is acquired by implementing inverse Fourier transform of the interference image. Then, the phase shifting method is applied to remove the complex-conjugate image. After all the cropped results are spliced side-by-side, the composite image for the whole depth range of the sample is completely achieved by shift-multiplexing CSD-OCT.

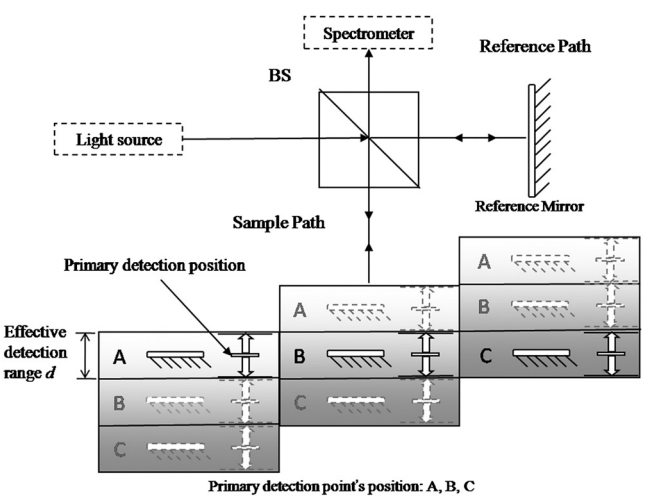

Fig. 2 The schematic diagram of the shift-multiplexing CSD-OCT. BS, beam splitter.

For implementing the tomographic imaging with the shift-multiplexing CSD-OCT, the parameters such as the initial position of the primary detection position, the shift spacing Δd, the effective detection range d, and the collecting times m at each primary detection position should be determined according to the requirement of detection. With respect to each of the primary detection positions arranged toward the depth from the sample's surface with equal spacing, every set of phase-shifted interference pattern is collected by CCD camera. As mentioned before, each set of phase-shifted interference patterns, the complex-conjugate image, and DC term of the tomographic imaging at each primary detection position should be eliminated by using the phase shifting method to obtain the tomographic image without any conjugate image and DC term. To avoid the complex-conjugate ambiguity of imaging, the four-step phase shift method with the phase shift angle of $\pi/2$ is used to remove complex-conjugate and DC terms in tomographic images. The conjugate-free tomographic images are cropped symmetrically around the center of each image by using the cropping parameter N to frame the cropping patterns of them. The cropping parameter N is dependent on the effective detection range. Based on the shift spacing Δd, the splicing parameter M can be calculated. All the cropped patterns are spliced into one composite tomographic pattern with the splicing parameter M, and thus the desired tomographic image for the targeted sample is achieved with shift-multiplexing CSD-OCT.

The cropping parameter N and the splicing parameter M are expressed as

$$N = \frac{2dn_1(\lambda_{\max} - \lambda_{\min})B}{\lambda_0^2 A}, \tag{1}$$

$$M = \frac{2\Delta dn_2(\lambda_{\max} - \lambda_{\min})B}{\lambda_0^2 A}, \tag{2}$$

where d is the effective detection range and Δd is the shift spacing, of which the values are taken according to the detection requirement. A is the horizontal pixel value of interference pattern on CCD, B is the horizontal pixel value of the conjugate-free tomographic image, λ_0 is the central wavelength of the near-infrared light emitted from an SLD source, $\lambda_{\max}$ and $\lambda_{\min}$ are maximum and minimum wavelengths of the SLD source, and n_1 and n_2 are the refractive indexes of the sample and air.

3 Experimental Results

To demonstrate the feasibility of the proposed method, we perform tomographic imaging for a target sample having layered structure. In our experimental setup of the shift-multiplexing CSD-OCT system, the two or three pieces of glass slides are stacked together one upon the other to form the layered structure of front and rear surfaces, which is employed as the target sample. In the first experiment, the target sample of 2.4 mm thickness consists of two-layer glass slides with a refractive index of ~1.5. The shift spacing of 500 μm is set, and then eight primary detection positions can be located by moving the sample stage with a shift spacing of 500 μm in the sample path.

According to Eqs. (1) and (2), the splicing parameter M is equal to the cropping parameter N since the optical length of effective detection range (in the sample) is taken as equal to the optical length between two adjacent primary detection positions (in the air) in the experiments. Accordingly, all the cropped images with the same pixel number can be accurately spliced side-by-side without the redundancy and deficiency of tomographic information. By calculation, the ratio of the shift spacing to effective detection range also makes sure that there is no redundancy or deficiency of tomogram.

The refractive index of air $n_2 = 1$ and the refractive index of the sample $n_1 = 1.5$, so we obtain the effective detection range as 500 μm/1.5 = 333.33 μm. For tomographic imaging over all the depth of the two-layer slides, eight interference patterns, each corresponding to the primary detection positions, are recorded by the CCD camera. After performing the above-mentioned technique, the recorded interference patterns are transformed into eight tomographic images. Then, the composite tomographic image of the two-layer slides is obtained by orderly assembly of the eight tomographic images together, each of them covering the effective detection range of 333.33 μm centered at each of the primary detection positions.

Figure 3 shows the result of tomographic imaging for the two-layer slides by shift-multiplexing CSD-OCT. The composite tomographic image of the two-layer slides is shown in Fig. 3(a), where the three bright lines are as follows: the first line shows the front surface of the first slide, the second line shows the rear surface of the first slide and the front surface of the second slide, and the third line shows the rear surface of the second slide, respectively, in order from top to bottom. Figure 3(b) shows the curve of the depth-dependent signal intensity corresponding to the composite tomographic image. In Fig. 3(b), three peaks each denote the front surface of the first slide, both the rear surface of the first slide and the front surface of second slide, and the rear surface of the second slide in order from left to right. And the real position of the sample's tomographic surface can be calculated by the peak's pixel position.

Similarly, the tomographic imaging result of the two-layer glass slides by CSD-OCT is shown in Fig. 4. As seen in Fig. 4(a), the center bright line on the tomographic image is the superposed surface of the two-layer glass slides. The image for the superposed surface is bright and clear, but it does not show clearly the front surface of the first slide and the rear surface of the second slide. Figure 4(b) is the curve of the depth-dependent signal intensity corresponding to the tomographic image. In Fig. 4(b), the signal peak indicates the position of the superposed surface formed by the rear surface of the first slide and the front surface of the second slide, and the signals marked out with dashed boxes denote the front surface of the first slide and the rear surface of the second slide, respectively. On comparing the signal intensities in the dashed boxes of Figs. 3(b) and 4(b), we find that the tomographic imaging by shift-multiplexing CSD-OCT is able to achieve more uniform signal intensity and higher axial sensitivity than that by CSD-OCT. Particularly, for large thickness of the target sample, the shift-multiplexing CSD-OCT system can perform the optimized tomographic imaging with more uniform brightness and clarity, as shown in Fig. 3(a).

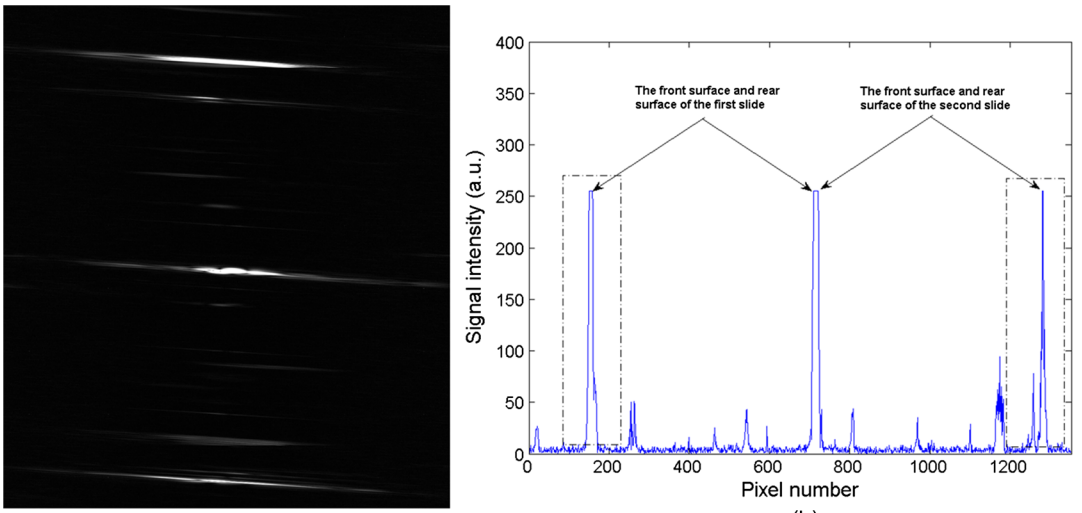

Fig. 3 The result of two-layer glass slides with shift-multiplexing CSD-OCT. (a) The composite tomographic image. (b) The curve of signal intensity. (The scaling parameter is taken as 3.1 μm optical path length per pixel.)

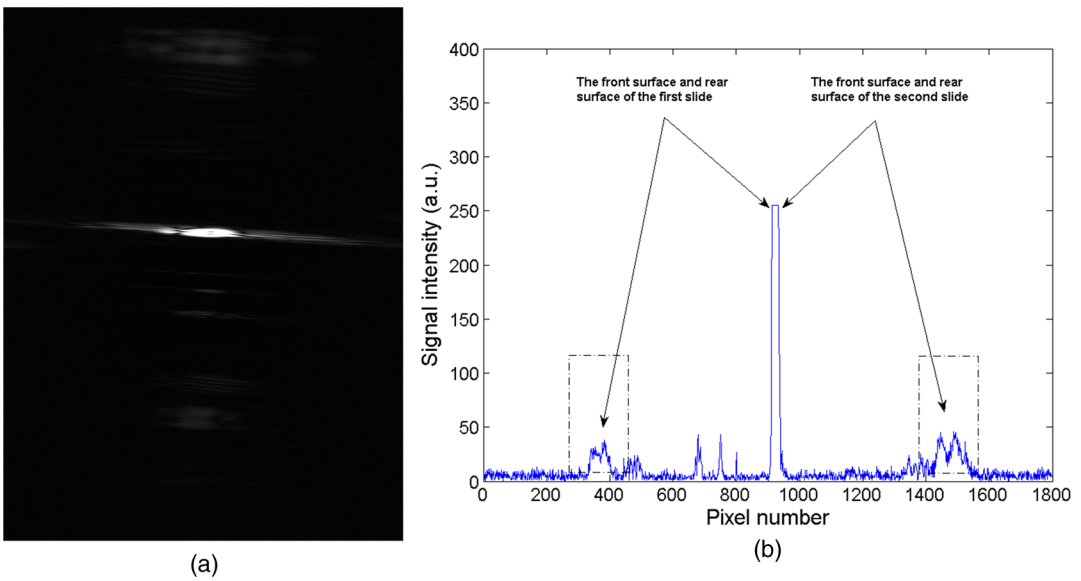

Fig. 4 The result of the two-layer glass slides with CSD-OCT. (a) The tomogram. (b) The curve of signal intensity. (The scaling parameter is taken as 3.1 μm optical path length per pixel.)

Moreover, for the thickness of the target sample larger than the maximum imaging depth of CSD-OCT system, our proposed method can effectively extend the detection depth. In the glass slides, the maximum image depth of our CSD-OCT system is ~3.1 mm. And the thickness of the two-layer glass slides is ~2.4 mm, which is less than the maximum detection depth of 3.1 mm. In the second experiment, the real thickness of the target sample consisting of three-layer glass slides is ~3.6 mm, which is greater than the maximum detection depth of our system for the glass media. Accordingly, the maximum detection depth of the CSD-OCT system is larger than the thickness of the two-layer glass slides, but is less than the thickness of the three-layer glass slides. Herein, the effective detection range, the shift spacing, and the phase shifting angle take the same values as those in the preceding experiment. Due to the increase of the detection range, 12 interference patterns are recorded by the CCD camera, corresponding to the 12 primary detection positions with equal spacing from the first inner surface of the sample, respectively. The composite tomographic image and the curve of depth-dependent signal intensity of three-layer glass slides are obtained by our proposed system, as shown in Fig. 5.

The four signal peaks from left to right of the curve in Fig. 5(b) indicate the measured signal intensities of the front surface of the first slide, the laminated layer of the rear surface of the first slide and the front surface of the second slide, the laminated layer of the rear surface of the second slide and the front surface of the third slide, and the rear surface of the third slide. Accordingly, all the layer structure

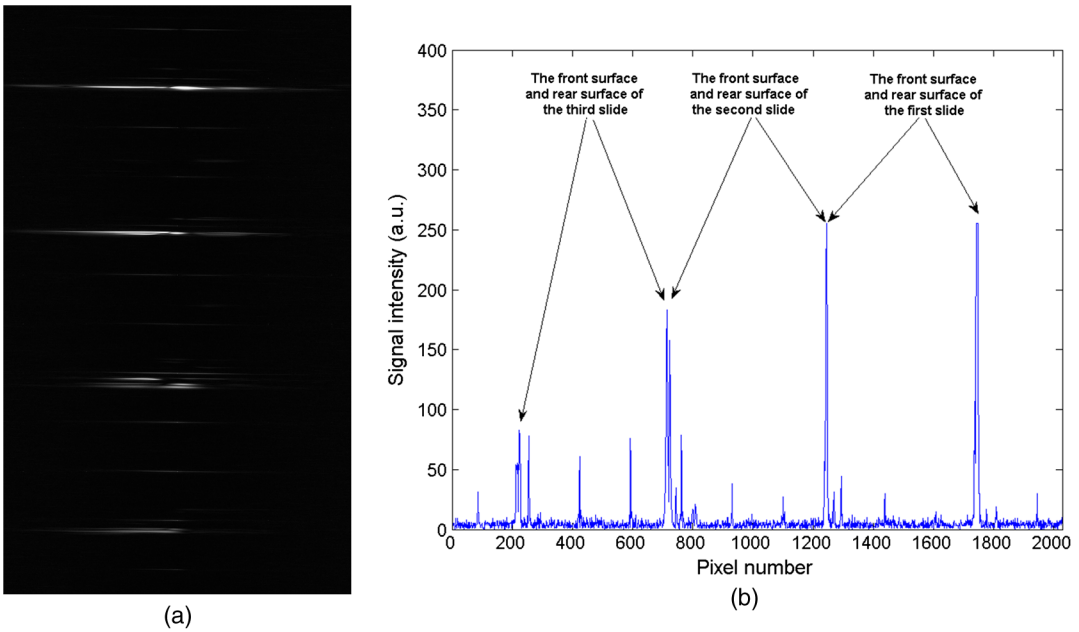

Fig. 5 The result of three-layer glass slides in shift-multiplexing CSD-OCT system. (a) The composite tomographic image. (b) The curves of signal intensity. (The scaling parameter is taken as 3.1 μm optical path length per pixel.)

information of the three-layer slides is yielded by using our proposed OCT system. The loss of the reflection light and transmission light is irresistible, which occurs in all the OCT detection processes. The light intensity of the reflected beam as a detection signal decreases with the penetration distance of transmission light into the sample because of the transmission loss and absorption loss. When the light beam reaches the fourth surface from the top to bottom, its light intensity gradually decreases, so that the light intensity of the incident beam into the fourth surface is the lowest. Thus, the intensity of the reflected light from the fourth surface is lower than any one of the other surfaces. The loss of the reflected light and transmission light depends on both the optical property and internal structure feature of the sample, and the wavelength of the light source. The shift-multiplexing CSD-OCT technique can deal with signal degradation of the system itself, but it is not applicable to reduce the light loss mentioned above.

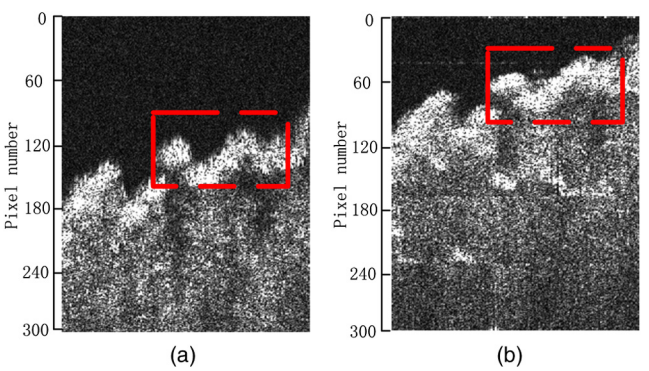

Fig. 6 The tomographic image of no-skin muskmelon (a) with CSD-OCT. and (b) with shift-multiplexing CSD-OCT. (The scaling parameter is taken as 3.1 μm optical path length per pixel.)

In the next experiment, a piece of muskmelon is used as a high scattering sample to be detected. The tomograms of a flesh slice of no-skin muskmelon with CSD-OCT and shift-multiplexing CSD-OCT methods are shown in Figs. 6(a) and 6(b), respectively, with the transverse scanning length of 6 mm (B-scan). We set the scanning speed of the system to ~10 Hz, and it takes 2 to 3 min for collecting and processing to get the detection result of the sample based on the performance of instruments. In our shift-multiplexing CSD-OCT setup, the tomographic image of no-skin muskmelon is obtained by assembling the cropping images at the five primary detection positions with the shift spacing of 250 μm and with B-scan detection. By comparing the images indicated with the dashed boxes in Figs. 6(a) and 6(b), we can observe a little better signal intensity of the no-skin muskmelon's flesh by shift-multiplexing CSD-OCT than by CSD-OCT.

The above experimental results show that the shift-multiplexing CSD-OCT can achieve an effective imaging for the large detection depth that is beyond the maximum imaging depth of CSD-OCT system.

4 Conclusion

We have proposed a new shift-multiplexing CSD-OCT system, the imaging depth of which is greatly extended by incorporating the shift-multiplexing detection positions with CSD-OCT technique. We also demonstrate experimentally the tomographic imaging with two-layer slides, three-layer slides, and no-skin muskmelon's flesh as the target samples with our proposed method. The results show that the shift-multiplexing CSD-OCT technique can achieve the optimized tomographic image with more uniform brightness and clarity for the different depth areas of a thick sample, and is effective for the tomographic imaging of larger detection depth beyond the maximum imaging depth of CSD-OCT system. From the results, it is concluded that

the shift-multiplexing CSD-OCT, as compared with CSD-OCT, can perform the desired detection even for increasing imaging depth without any change of instruments in the OCT system.

Moreover, the parameters of shift spacing and effective detection range can be selectively valued according to the required detection, and thus this method is flexible to detect the continuous or separated areas of the target sample. Additionally, by considering that imaging sensitivity declines observably with the detected region away from the position of the mirror's virtual image, a higher sensitivity area near the DC term in a tomographic image can be fully utilized to achieve tomographic imaging with more uniform brightness and clarity by shift-multiplexing CSD-OCT. In a practical application, the trade-off between the sensitivity and the time-consumption should be considered. But it will not waste much time to move the primary detection points. In the above experiments, the movement of primary detection point consumes ~0.5 s, which is at the scanning speed's order of magnitude, so we think it is acceptable. The shift-multiplexing CSD-OCT technique can be promisingly used in multilayer optical disc readout, jewelry identification, solutions or liquor detection, and so on. In these areas, it is commonly required to increase imaging depth for the detection object. Thus, we can say that the shift-multiplexing CSD-OCT has a great potential to extend detection depth for tomographic imaging and to enhance the flexibility of detection in the applications of OCT.

Acknowledgments

This work is supported by The Science Foundation of Education Commission of Beijing under Grant No. KZ201310005007 and Graduate Technology Fund of Beijing University of Technology under Grant No. ykj-2013-9357.

References

1. D. Huang et al., "Optical coherence tomography," *Science* **254**(5035), 1178–1181 (1991).
2. J. Jang et al., "Complex wavefront shaping for optimal depth-selective focusing in optical coherence tomography," *Opt. Express* **21**(3), 2890–2902 (2013).
3. R. Leitgeb, C. K. Hitzenberger, and A. F. Fercher, "Performance of Fourier domain vs time domain optical coherence tomography," *Opt. Express* **11**(22), 889 (2003).
4. P. Xi et al., "Evaluation of spectrometric parameters in spectral-domain optical coherence tomography," *Appl. Opt.* **50**(3), 366–372 (2011).
5. Z. Ding et al., "High-resolution optical coherence tomography over a large depth range with an axicon lens," *Opt. Lett.* **27**(4), 243–245 (2002).
6. L. An et al., "High-resolution 1050 nm spectral domain retinal optical coherence tomography at 120kHz A-scan rate with 6.1 mm imaging depth," *Biomed. Opt. Express* **4**(2), 245–259 (2013).
7. Y. Yang et al., "Development of full-field optical coherence tomography system," *Acta Phys. Sin.* **58**(3), 1773–1778 (2009).
8. M. Wojtkowski et al., "Full range complex spectral optical coherence tomography technique in eye imaging," *Opt. Lett.* **27**(16), 1415–1417 (2002).
9. T. Fabritius et al., "Complex conjugate resolved retinal imaging by one-micrometer spectral domain optical coherence tomography using an electro-optical phase modulator," *J. Opt. Soc. Korea* **15**(2), 111–117 (2011).
10. P. Bu, X. Wang, and O. Sasaki, "Dynamic full-range Fourier-domain optical coherence tomography using sinusoidal phase-modulating interferometry," *Opt. Eng.* **46**(10), 105603 (2007).
11. R. Leitgeb et al., "Phase-shifting algorithm to achieve high-speed long-depth-range probing by frequency-domain optical coherence tomography," *Opt. Lett.* **28**(22), 2201–2203 (2003).
12. S. Zotter et al., "Sample motion-insensitive, full-range, complex, spectral-domain optical-coherence tomography," *Opt. Lett.* **35**(23), 3913–3915 (2010).
13. B. Baumann et al., "Full range complex spectral domain optical coherence tomography without additional phase shifters," *Opt. Express* **15**(20), 13375 (2007).
14. B. Braaf et al., "Phase-stabilized optical frequency domain imaging at 1 μm for the measurement of blood flow in the human choroid," *Opt. Express* **19**(21), 20886–20903 (2011).
15. K. Zhang, Y. Huang, and J. Kang, "Full-range Fourier domain optical coherence tomography imaging probe with a magnetic-driven resonant fiber cantilever," *Opt. Eng.* **50**(11), 119002 (2011).
16. E. Götzin et al., "High speed full range complex spectral domain optical coherence tomography," *Opt. Express* **13**(2), 583–594 (2005).
17. H. Cheng and M. Shiu, "Experimental demonstration of high-speed full-range Fourier domain optical coherence tomography imaging using orthogonally polarized light and a phase-shifting algorithm," *Appl. Opt.* **51**(36), 8762–8768 (2012).
18. P. Targowski et al., "Complex spectral OCT in human eye imaging in vivo," *Proc. SPIE* **5140**, 28–32 (2003).
19. Y. Tao, M. Zhao, and J. Izatt, "High-speed complex conjugate resolved retinal spectral domain optical coherence tomography using sinusoidal phase modulation," *Opt. Lett.* **32**(20), 2918–2920 (2007).
20. Z. Wang et al., "Increasing the imaging depth of spectral-domain OCT by using interpixel shift technique," *Opt. Express* **14**(16), 7014–7023 (2006).
21. Y. Zhang et al., "Time-domain interpolation for Fourier-domain optical coherence tomography," *Opt. Lett.* **34**(12), 1849–1851 (2009).
22. M. Szkulmowski et al., "Flow velocity estimation using joint spectral and time domain optical coherence tomography," *Opt. Express* **16**(9), 6008–6025 (2008).
23. M. Szkulmowski et al., "Flow velocity estimation by complex ambiguity free joint spectral and time domain optical coherence tomography," *Opt. Express* **17**(16), 14281–14297 (2009).
24. I. Grulkowski et al., "Velocity resolution and minimum detectable velocity in joint spectral and time domain OCT," in *Biomedical Optics and 3-D Imaging*, OSA Technical Digest (CD), paper BTuD18, Optical Society of America, Miami, Florida (2010).
25. M. Szkulmowski and M. Wojtkowski, "Averaging techniques for OCT imaging," *Opt. Express* **21**(8), 9757–9773 (2013).

Haochong Huang received BS degrees in applied physics in 2007 from Beijing University of Technology, China. Now he is a PhD candidate (Master-Doctor combined program) in optical engineering in the Beijing University of Technology, China. His main research interests are optical coherence tomography and digital holography.

Biographies of the authors are not available.